MBoC | ARTICLE

Local RhoA activation induces anillin-independent septin recruitment in interphase cells

Shreya Chandrasekar, Margaret E. Utgaard, Bradley Somerfield, Huini Wu, Jordan R. Beach*, and Patrick W. Oakes*

Deptartment of Cell and Molecular Physiology, Loyola University Chicago, Stritch School of Medicine, Maywood, IL 60153

ABSTRACT **The regulation of the actin cytoskeleton is key to controlling cell shape and structure. While the Rho GTPase RhoA is well known to regulate the actomyosin cytoskeleton, its function in controlling the septin cytoskeleton remains unclear. As RhoA interactions can vary in both time and space, they can be challenging to discern from traditional bulk biochemical assays. Here, we use multiple optogenetic tools to spatially and temporally increase myosin localization, stimulate contractile force, and activate RhoA to investigate how RhoA and its downstream effector myosin impact the septin cytoskeleton. We find that neither local accumulation of myosin nor increased activity of myosin is sufficient to alter septin architecture. Local activation of RhoA, however, results in a local increase in septin accumulation. Importantly, this septin increase is independent of the scaffolding protein anillin, which can directly bind both septin and RhoA. Together, these data expand the potential role of septins in mediating RhoA signaling by stimulating the remodeling of the septin cytoskeleton.**

SIGNIFICANCE STATEMENT

- Septins are cytoskeletal filaments that play a key role in cell division, where RhoA is the dominant signaling mechanism. During interphase, they decorate a subpopulation of the stress fibers in the cytoskeleton, but the mechanisms regulating their localization remain unclear.
- We use optogenetic tools to show that RhoA activation, and not just its downstream effector myosin or contractility, stimulates septin recruitment locally.
- This work suggests that septins could play a significant role in mediating RhoA signaling and coordinating remodeling throughout the cytoskeleton.

Monitoring Editor
Elizabeth Chen
University of Texas
Southwestern Medical Center

Received: Sep 29, 2025
Revised: Mar 16, 2026
Accepted: Mar 20, 2026

This article was published online ahead of print in MBoC in Press (http://www.molbiolcell.org/cgi/doi/10.1091/mbc.E25-09-0468) on March 25 2026.

Author contributions: SC, JRB and PWO conceived the study. SC and MEU performed experiments and data analysis. BS, MEU, HW and JRB provided critical cell lines and reagents. SC, JRB and PWO wrote the manuscripts with critical feedback from co-authors.

Conflicts of interest: The authors declare no competing financial interest.

*Address correspondence to: Jordan R. Beach (jbeach1@luc.edu); Patrick W. Oakes (poakes@luc.edu).

Abbreviations used: NM2A, non-muscle myosin 2A; MLCK, Myosin Light Chain Kinase; TFM, Traction Force Microscopy; iLID, improved light inducible dimer; ROCK, rho-associated coiled-coil containing protein kinase; RLC, regulatory light chain; LOV, light oxygen voltage; GEF, guanine nucleotide exchange factor; LARG, leukemia-associated rhoA-specific GEF

INTRODUCTION

The cytoskeleton plays a key role in determining cell shape, which in turn is intimately connected to cell behavior. Cytoskeletal networks, in conjunction with their associated binding proteins and motors, dynamically assemble and reorganize in response to a variety of biochemical and mechanical signals to produce specific architectures. This is especially true for the actin and myosin cytoskeleton, the dominant architectural element in cells (Svitkina, 2018).

The Rho family of GTPases (RhoA, Rac, and Cdc42) often act between upstream cues and downstream actomyosin rearrangement, functioning as master regulators of the cytoskeleton (Jaffe and Hall, 2005). The spatial and temporal activation of Rho GTPases coupled with their mutual antagonism enables critical cellular processes like migration and cell division (Lawson and Ridley, 2018; Müller *et al.*, 2020). Rho GTPases signal by binding and activating downstream effectors. For example, GTP-bound RhoA can activate formins to induce actin polymerization and bind to Rho-associated coiled-coil containing protein kinase (ROCK) to phosphorylate and activate myosin 2, thereby driving actomyosin activity (Ridley and Hall, 1992; Shizaki *et al.*, 1997; Watanabe *et al.*, 1997). Actomyosin contractility can then actuate mechanical responses by other cytoskeletal elements and feedback to influence Rho GTPases (Bhadriraju *et al.*, 2007; Bement *et al.*, 2015). This dynamic Rho-driven mechanical crosstalk model likely influences all cytoskeletal elements, but has been largely unexplored in the septin cytoskeleton.

Septins are GTP-binding proteins that polymerize to form cytoskeletal filaments and are broadly conserved (Mostowy and Cossart, 2012; Woods and Gladfelter, 2021; Delic *et al.*, 2024). In mammals, there are 13 septin genes divided into four families based on sequence homology, with members of each family showing tissue-specific expression (Dolat *et al.*, 2014a). Mammalian septins oligomerize into nonpolar palindromic subunits consisting of either six or eight monomers drawn from three or four families, respectively (Cavini *et al.*, 2021). These hexamers and octomers then polymerize into filaments and other higher-order structures (Kinoshita *et al.*, 2002; Jiao *et al.*, 2020). First discovered as critical components of cytokinesis in budding yeast (Hartwell, 1971), septins play important roles across physiology, including cell migration (Shindo and Wallingford, 2014; Dolat *et al.*, 2014b; Gabbert *et al.*, 2023), neurogenesis (Ageta-Ishihara and Kinoshita, 2021), immunology (Tooley *et al.*, 2009; Zhovmer *et al.*, 2024), host-pathogen interactions (Van Ngo and Mostowy, 2019), and ciliogenesis (Palander *et al.*, 2017). Furthermore, knockout of multiple individual septin genes is embryonically lethal (Röseler *et al.*, 2011; Füchtbauer *et al.*, 2011; Menon *et al.*, 2014) and changes in septin expression are linked to several diseases, including Alzheimer's and breast cancer (Peterson and Petty, 2010; Devlin *et al.*, 2021; Weems *et al.*, 2023), demonstrating a critical role for septins throughout cell biology.

Septins are largely considered protein scaffolds based on their ability to interact with the plasma membrane and multiple cytoskeletal proteins, in addition to their lack of associated motors. At the plasma membrane, septin distribution is heterogeneous as septins exhibit a preference for membranes with micron-scale curvature (Bridges *et al.*, 2016; Cannon *et al.*, 2019; Nakazawa *et al.*, 2023). In vitro, septins can directly bind both microtubules and actin to induce bundling (Bai *et al.*, 2013; Mavrakis *et al.*, 2014). In cells, however, these interactions are more complicated as septins decorate only subpopulations of both actin and microtubule networks (Spiliotis, 2018). Furthermore, a previous report suggested septins could also bind directly to nonmuscle myosin 2A (NM2A; Joo *et al.*, 2007). Together, these features make septins prime conduits to translate both biochemical and biophysical signals in cells.

While pharmacological and genetic perturbations can globally perturb septin function, it is clear that septin localization in vivo is regulated both spatially and temporally. Cdc42 signaling has previously been shown to play a prominent role in septin regulation (Joberty *et al.*, 2001; Gladfelter *et al.*, 2002; Schmidt and Nichols, 2004; Salameh *et al.*, 2021; Tomasso *et al.*, 2025). However, septin's essential role in the mammalian contractile ring, where RhoA is the dominant signaling mechanism and actomyosin is the dominant architectural element (Carim and Hickson, 2023), suggests septins may respond to additional biochemical inputs. Septins have also been broadly implicated in cell mechanics (Lam and Calvo, 2018; Vadnjal *et al.*, 2022), which is largely mediated by RhoA signaling, although their precise contribution remains uncertain. This link to cytokinesis and mechanics, coupled with in vitro actin binding and possible myosin 2 binding, compelled us to more carefully dissect the spatiotemporal contribution of actin, myosin 2, and RhoA in septin network formation.

Like other cytoskeletal elements, septin networks are both dynamic and heterogeneous (Schmidt and Nichols, 2004; Hagiwara *et al.*, 2011; Martins *et al.*, 2023). Optogenetic tools, therefore, are particularly well-suited to spatiotemporally probe regulation of septin networks. These tools take advantage of light-sensitive proteins that change conformation when exposed to light of certain wavelengths (Kramer *et al.*, 2021; Chandrasekar *et al.*, 2023). The improved light-inducible dimerization (iLID) system is a popular version of this approach based on its specificity, rapid association and dissociation kinetics, and need for minimal intensity of light for activation (Guntas *et al.*, 2015; Natwick and Collins, 2020). In particular, these tools have proven adept at locally stimulating GTPase signaling by recruiting specific guanine exchange factors (GEFs) to activate RhoA, Rac, or Cdc42 (Wagner and Glotzer, 2016; O'Neill *et al.*, 2016; Valon *et al.*, 2017; de Beco *et al.*, 2018; Inaba *et al.*, 2021; Mahlandt *et al.*, 2023b).

Here, we set out to investigate a role for RhoA signaling in regulating septin accumulation in interphase cells. We first demonstrate that inhibition of RhoA or myosin 2, a downstream effector of RhoA, results in septin relocalization from actin stress fibers to the plasma membrane. We next show that optogenetic recruitment of myosin 2 alone is insufficient to alter septin localization. Similarly, optogenetic activation of myosin to locally increase contraction via recruitment of myosin light chain kinase (MLCK) also fails to induce septin recruitment. Local activation of RhoA, however, results in a local increase of septin in an anillin-independent manner. Combined, these data suggest that RhoA signaling, and not just contractility, is able to induce septin assembly, expanding the reach of septins in these critical biochemical signaling networks.

RESULTS

Local recruitment of myosin 2 is not sufficient to recruit septins

As septins and myosin 2 colocalize at the contractile ring and have also been previously reported to interact (Joo *et al.*, 2007), we set out to test whether inhibiting either RhoA or its downstream effector myosin 2 would impact septin localization. We found that

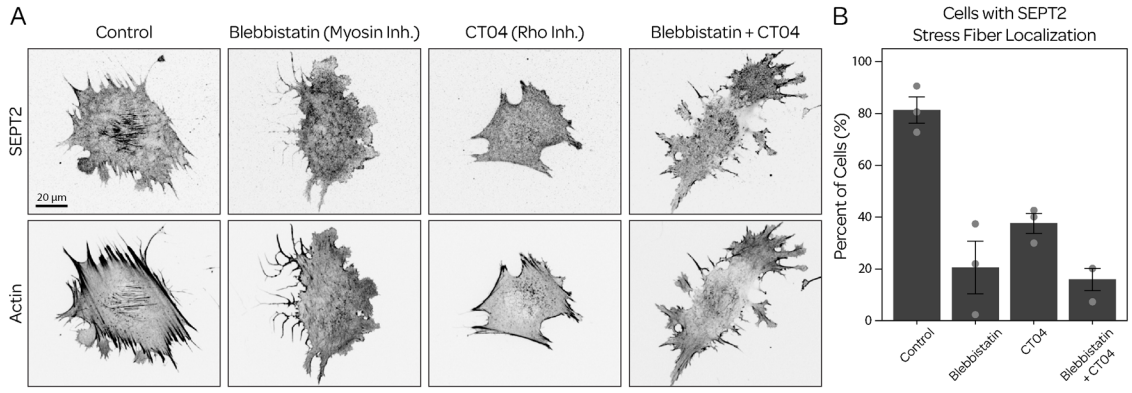

FIGURE 1: Inhibition of myosin or Rho leads to reduced SEPT2 accumulation on stress fibers. (A) Representative fixed fibroblasts stained with a SEPT2 antibody and phalloidin in the presence of the myosin inhibitor blebbistatin, the Rho inhibitor CT04, or a combination of the two. (B) The percent of cells showing SEPT2 localization to stress fibers in each of the conditions. Grey dots represent the average value with at least 55 cells per condition, per repeat ($n = 3$).

treating fibroblasts with either a C3 Transferase-derived inhibitor of RhoA (CT04) or the myosin 2 inhibitor blebbistatin resulted in disassembly of central septin stress fiber networks and increased accumulation of septins at the plasma membrane (Figure 1, A and B). Combining the two drug treatments showed no additive effect. As this implies that myosin may regulate septin localization, we set out to directly test whether recruitment of myosin 2 would result in increased septin accumulation. We recently developed an iLID-based tool to use light to locally recruit myosin 2 (Quintanilla *et al.*, 2024). Briefly, this iLID optogenetic system consists of a transmembrane anchor (Stargazin) attached to a light-oxygen-voltage sensing domain (LOV2) whose Jα helix has been modified with a small bacterial peptide (SsrA), which remains masked in the dark state (Guntas *et al.*, 2015; Natwick and Collins, 2020; Figure 2A). Upon blue light ($\lambda < 500$ nm) exposure, the Jα helix unfolds, exposing the SsrA peptide and allowing it to bind its complementary binding partner SspB attached to NM2A (Figure 2A; Quintanilla *et al.*, 2024).

Consequently, local illumination in a region spanning the cell resulted in a significant increase in myosin intensity that abated when the stimulating light was removed (Figure 2, B–E; Supplemental Movie S1). However, we saw no appreciable change in septin intensity or localization in response to the increasing density of myosin (Figure 2, B–E; Supplemental Movie S1).

Interestingly, while we previously found myosin 2 recruitment self-stimulated myosin filament assembly in the lamella where myosin filaments were initially sparse (Quintanilla *et al.*, 2024), here we saw an increase in intensity of myosin but minimal changes in architecture when recruiting to regions where myosin 2 filaments were already abundant. To check whether the increase in myosin impacted the overall contractility of the cell, we used traction force microscopy (TFM) to measure cellular force production. As forces generated in the cytoskeleton are transmitted to the substrate via focal adhesions, local changes in contractility in the cytoskeleton can alter traction stress measurements outside the region of recruitment (Oakes *et al.*, 2017). We therefore measured the total contractile work performed by the cell, normalized by the cell area, which we have shown previously is a better reporter of cell contractility (Oakes *et al.*, 2014). Interestingly, we found that despite the increase in myosin in these regions, the total contractile work performed did not change (Figure 2, F and G; Supplemental Movie S2). Myosin accumulation alone is thus insufficient to induce septin accumulation or contractility.

Locally inducing contraction does not alter septin localization

While our data suggest that myosin is not directly interacting with septins, the septin rearrangement we observed upon myosin inhibition (Figure 1) suggests that myosin contractile activity could still aid in septin localization. We therefore sought to increase local myosin contractile activity by modulating its phosphorylation. To achieve this we swapped the stargazin anchor in our iLID system with myosin regulatory light chain (RLC), and attached the SspB to the catalytic domain of myosin light chain kinase (MLCK; Figure 3A; Supplemental Figure S1; Supplemental Movie S3). This tool should therefore stimulate both RLC Thr18/Ser19 phosphorylation on myosin monomers to induce nascent filament formation, and simultaneously increase the RLC phosphorylation in existing filaments to preserve/prolong their activity (Figure 3A). To validate this approach, we again measured the total contractile work performed by the cell using TFM (Figure 3B; Supplemental Movie S4). We saw a steady increase in traction forces and the overall contractile work performed by the cell in response to local recruitment of MLCK to myosin, which decreased as the stimulating light was removed (Figure 3C). This demonstrates that recruitment of the catalytic domain of MLCK to myosin results in increased contractility.

While the traction stresses largely increased outside the region of MLCK recruitment due to tension propagating along actin fibers to focal adhesions, inside the recruitment region, we saw a local increase in signal of the Sspb-MLCK (Figure 3, B–G; Supplemental Movie S5). This indicates that within the cytoskeleton, contractility and tension should be increasing locally within the recruitment region where the MLCK is acting on myosin. To test whether an increase in local contraction impacts septins, we repeated our local MLCK recruitment while visualizing septins. We found that increasing contractility was not sufficient to drive septin recruitment, as we did not see any significant changes in septin intensity in the region of MLCK recruitment (Figure 3, D–G; Supplemental Movie S5). These data suggest that myosin-based contractility is not sufficient to recruit or alter septin localization in interphase cells.

Local recruitment of LARG-DH specifically activates RhoA

Since increased myosin accumulation and contractility alone are insufficient to recruit septins, additional signaling must be necessary. Septins are prominently found in the contractile ring during cytokinesis (Longtine *et al.*, 1996; Carim and Hickson, 2023). In this critical structure, there is both local elevation of RhoA signaling

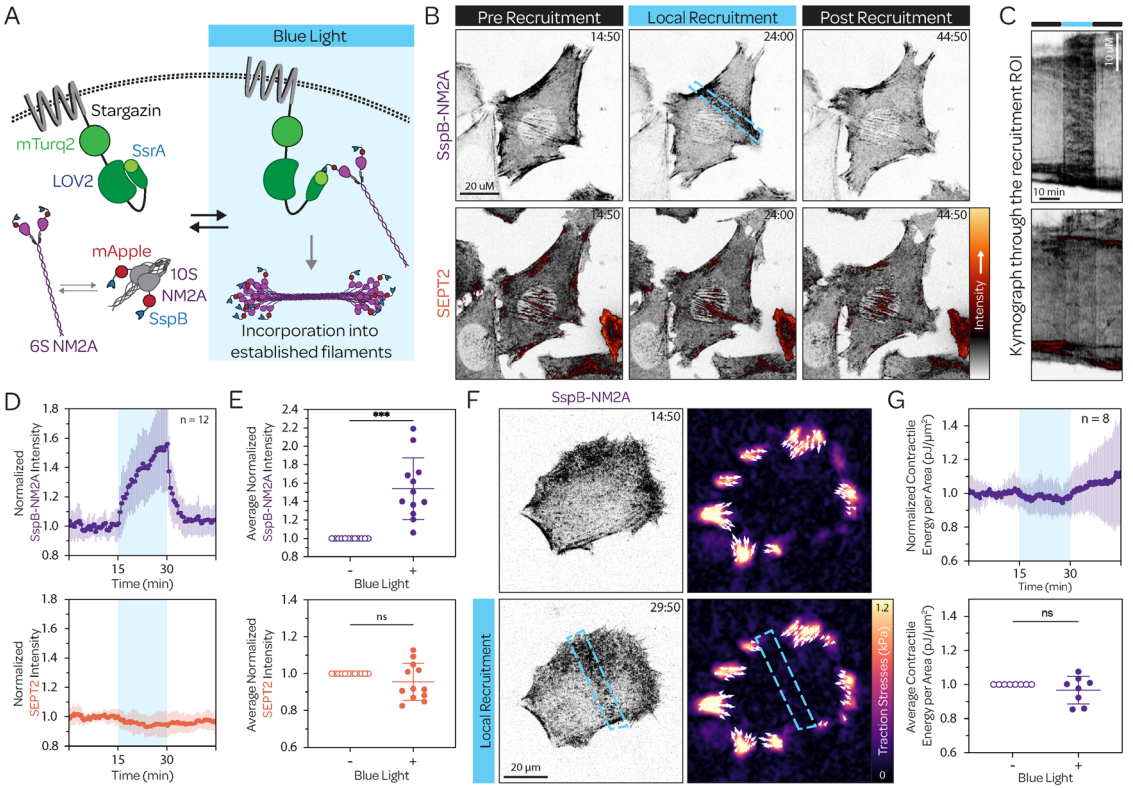

FIGURE 2: Local recruitment of myosin 2 is not sufficient to recruit septins. (A) A schematic of the tool to locally recruit myosin. A LOV2-SsrA molecule and mTurq2 fluorophore are anchored to the plasma membrane via stargazin. Simultaneously, an NM2A construct tagged with an mApple-SspB is expressed in the cytosol. Upon local blue light stimulation (blue box), the SspB-mApple-NM2A is recruited to the plasma membrane, where it can enhance filament assembly. When blue light is removed, the two components disassociate. (B) Representative images of a Halo-labeled SEPT2-Halo fibroblast expressing the SspB-mApple-NM2A, immediately before, during, and after local recruitment (blue dashed box; see Movie S1). (C) A kymograph drawn through the activation region shows increased NM2A intensity but no change in SEPT2 intensity during the activation period. (D) Average SspB-mApple-NM2A and SEPT2-Halo intensities (mean ± SD) over time in the recruitment region, normalized to the pre-recruitment time points. The recruitment period is indicated by the blue background. (E) Scatter plots of average intensity changes in the recruitment region between the 50 s pre-recruitment and the final 50 s of recruitment per cell. (F) Representative images of myosin and the accompanying traction stress maps before and during local myosin recruitment (refer to Supplemental Movie S2). (G) Average measurements of the normalized total contractile work per area performed by cells over time, and scatter plots comparing the contractile work per area between the 50 s pre-activation and the final 50 s of activation per cell. * and *** indicate $p \leq 0.05$ and ≤ 0.001, respectively. n values indicate the number of cells analyzed.

(Wagner and Glotzer, 2016) and an increase in anillin, a scaffolding protein that can bind both septin and active RhoA (Hickson and O'Farrell, 2008). We thus set out to investigate whether these proteins contribute to septin organization and accumulation in interphase cells.

RhoA is regulated by the activity of multiple guanine nucleotide exchange factors (GEFs) and GTPase-activating proteins (GAPs), which can target either individual or multiple RhoGTPases (Guilluy *et al.*, 2011). Multiple optogenetic probes to control RhoA activation have been developed, targeting either specific GEFs or RhoA itself. Leukemia-associated Rho GEF (LARG; also known as ARHGEF12) is a RhoA-specific GEF (Jaiswal *et al.*, 2011). Previous works have shown that optogenetically recruiting the DH domain from LARG is sufficient to activate RhoA locally and stimulate downstream actin polymerization, myosin phosphorylation, and force production (Supplemental Figure S2, A and B; Wagner and Glotzer, 2016; Oakes *et al.*, 2017; Inaba *et al.*, 2021; Seze *et al.*, 2023). As previous studies have shown that Cdc42, another Rho GTPase, and its downstream effectors can regulate septin formation (Joberty *et al.*, 2001; Calvo *et al.*, 2015), we first confirmed that the truncated LARG- DH maintained its specificity for RhoA and did not also activate Cdc42. Using an iLID system again anchored to the plasma membrane, we locally recruited SspB-LARG-DH while simultaneously using biosensors to measure either RhoA (Supplemental Figure S2, C–F; Supplemental Movie S6) or Cdc42 activity (Supplemental Figure S2, G–J; Supplemental Movie S7). While recruitment of LARG-DH reliably increased local RhoA activity, we saw no similar increase in Cdc42 activity (Supplemental Figure S2, C–J), indicating that the truncated LARG retains its specificity for RhoA.

Local RhoA activation does not result in anillin recruitment

We next investigated whether local RhoA activation results in recruitment of anillin, which plays a key role in coordinating the actomyosin contractile ring formation (Hickson and O'Farrell, 2008; Carim and Hickson, 2023). Anillin contains a Rho-binding domain,

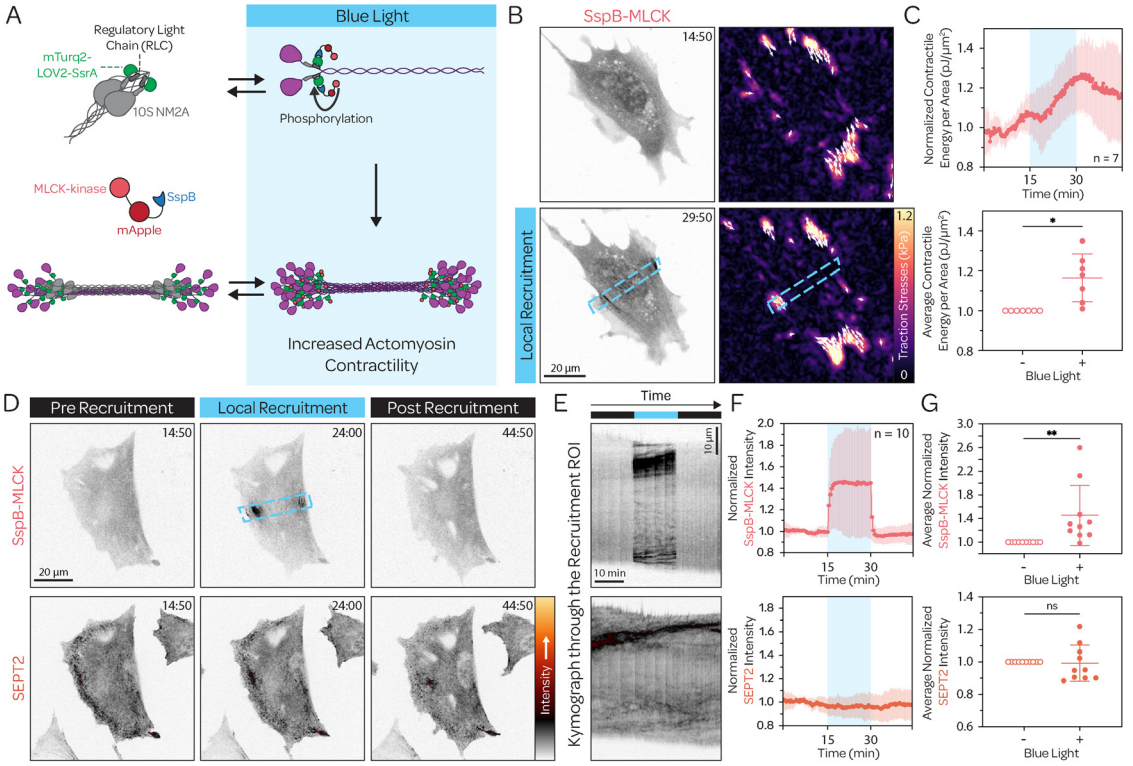

FIGURE 3: Local recruitment of MLCK to myosin filaments elevates contractility but does not alter septin localization. (A) A schematic of the optogenetic MLCK tool used to increase myosin-based contractility. The LOV2-SsrA molecule was anchored to the myosin RLC while the catalytic domain of MLCK tagged with SspB-mApple was expressed in the cytosol. Upon blue light illumination, SsrA-SspB binding should result in increased activation of myosin by the recruitable MLCK. When the blue light is turned off, MLCK dissociates from the myosin RLC. (B) Representative images of a fibroblast expressing the Sspb-mApple-MLCK and the corresponding traction maps before and during local recruitment (blue dashed box; see Supplemental Movie S4). (C) Average measurements of the normalized total contractile work per area performed by cells, and scatter plots comparing the contractile work per area before and during activation (mean ± SD). (D) Representative images of a SEPT2-Halo fibroblast expressing SspB-mApple-MLCK immediately before, during, and after local stimulation (blue dashed box; refer to Supplemental Movie S5). (E) Kymograph drawn through the region of recruitment in the cell shown in (D). (F) Normalized SspB-mApple- MLCK (top) and SEPT2-Halo (bottom) intensities (mean ± SD) over time in the region of recruitment, with recruitment periods indicated by the blue background. (G) Scatter plots of average intensity changes in the recruitment regions between the 50 s pre-recruitment and the final 50 s of recruitment per cell (mean ± SD). ns, *, and ** indicate $p > 0.05$, ≤ 0.05, and ≤ 0.01, respectively. n values indicate the number of cells analyzed.

a septin-binding domain, and a pleckstrin homology (PH) domain on its C-terminus, and myosin and actin binding domains on its N-terminus (Hickson and O'Farrell, 2008). Anillin expression is highly correlated with the cell-cycle (Field and Alberts, 1995; Zhao and Fang, 2005; Mahdessian *et al.*, 2021), but when expressed is thought to reside primarily in the nucleus before nuclear envelope breakdown. Recent results, however, have suggested that it may also have some cytoplasmic roles outside of cell division (Tran *et al.*, 2025). We first fixed and stained cells to compare anillin expression between cells in interphase and during cytokinesis. The residual anillin expression in interphase relative to cytokinesis was primarily restricted, when present, to the nucleus (Figure 4A). To test whether local recruitment of RhoA resulted in increased anillin recruitment in interphase cells, we locally activated RhoA and fixed after 15 min of activation, a time point consistent with our other optogenetic experiments (Figure 4B). Anillin signal remained unchanged in interphase cells where local RhoA was activated (Figure 4B), from which we conclude that interphase recruitment of LARG-DH activates RhoA without significantly modulating any cytoplasmic anillin.

Local RhoA activation induces septin recruitment

Having confirmed that local recruitment of LARG-DH should activate only RhoA, we set out to investigate whether RhoA activation would impact septin localization. To test this, we locally activated RhoA and measured changes in SEPT2 intensity in the region of activation (Figure 5, A–E). In contrast to the LARG-DH, which shows a rapid increase, we routinely saw that activation of RhoA resulted in a slower accumulation of septin into the activation region (Figure 5, A–D; Supplemental Movie S8). During the 15 min activation period, septin intensity progressively and significantly increased by ~20% and decreased when the stimulating light was turned off (Figure 5, C–E). Since RhoA activation leads to downstream actin polymerization and myosin phosphorylation, which combine to increase force production, we sought to test whether activation of RhoA resulted in a significantly larger increase in contractility than the local recruitment of MLCK. Using TFM, we locally activated RhoA and observed an ~15%–20% increase in the contractile work being performed by the cell (Figure 5, F and G; Supplemental Movie S9), similar to the increase we observed when locally recruiting MLCK (Figure 3C). Together, these data suggest that local RhoA activation recruits

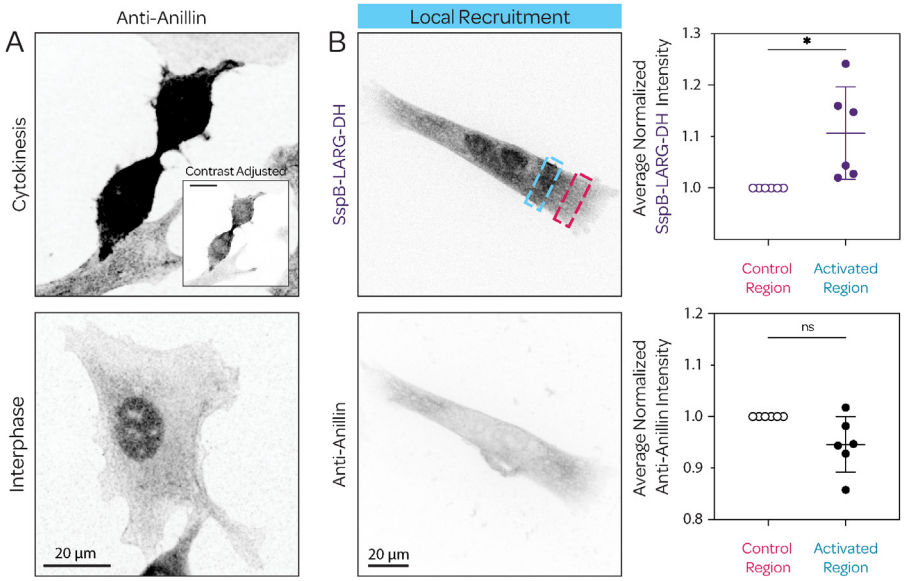

FIGURE 4: Local RhoA activation does not result in anillin recruitment (A) Fibroblasts were fixed and stained with an anti-anillin antibody during cytokinesis and interphase. Images are shown with identical contrast settings. Inset is a contrast-adjusted image to show that anillin expression is increased at the midbody as expected during cytokinesis. (B) Representative fibrob- last stably expressing Stargazin-mTurq2-LOV2-SsrA and transiently expressing mScarlet-SspB-LARG-DH (top), fixed during local activation of RhoA and stained with anti-anillin (bottom). (C) Scatter plots showing differences in average fluorescence intensity between the light-activated region (blue box) and an adjacent non-activated region (red box). ns and * indicate $p > 0.05$ and ≤ 0.05, respectively.

septins through a mechanism specific to RhoA and its possible downstream effectors, rather than simply by increasing contractility.

DISCUSSION

While the role of septins in cell division has been clearly defined, their functions during the rest of the cell cycle are more varied. It has long been reported that septins colocalize and interact with the actomyosin cytoskeleton (Kinoshita *et al.*, 2002), leading to suggestions that septins are responding to myosin-generated forces (Lam and Calvo, 2018). Our data shows that inhibition of myosin or RhoA causes septins to relocalize from stress fibers to the cortex (Figure 1), but that reciprocal experiments increasing myosin concentration (Figure 2) or contractility (Figure 3) are insufficient to alter septin filament localization independent of RhoA. In contrast, local activation of RhoA robustly promoted septin recruitment at the site of activation (Figure 5) in an anillin-independent manner (Figure 4). These data highlight that RhoA activity provides an alternative signaling pathway to lead to septin recruitment.

Given septin's appearance on stress fibers and other actin structures in the cell (Kinoshita *et al.*, 2002; Dolat *et al.*, 2014b; Martins *et al.*, 2023; Sturgess *et al.*, 2024), the potential for crosstalk between septin and myosin has been a tantalizing hypothesis. Previous work suggested that SEPT9 and myosin may compete for similar actin binding sites (Smith *et al.*, 2015), while other work suggested that SEPT2 can directly bind myosin (Joo *et al.*, 2007). While it is clear that septin and myosin can be in proximity on actin filaments, our data do not support either a direct interaction or competition for sites, as we see neither an increase nor a decrease in septin intensity upon local myosin 2 recruitment. As these previous studies both used purified proteins, it is possible that in the cell, the presence of additional actin-binding proteins and signaling partners limits their direct interactions. This would be consistent with the presence of anillin to act as a scaffold for these two proteins during cell division (Hickson and O'Farrell, 2008), and with other recent work showing that Bni5 in yeast performs a similar function (Okada *et al.*, 2023). It is also possible that septin and myosin are regulated independently despite their colocalization, as was recently demonstrated in Drosophila border cell clusters (Gabbert *et al.*, 2023).

On the signaling side, Rho family GTPases are obvious candidates to contribute to septin regulation given their strong impact on actin dynamics and architectures. Previous works established that Cdc42 and its downstream effectors, BORGs, can impact septin behavior (Joberty *et al.*, 2001; Gladfelter *et al.*, 2002; Calvo *et al.*, 2015, 2016; Salameh *et al.*, 2021). Given the prominent role of both RhoA and septins in cell division, however, the possibility of a RhoA-septin signaling axis seems reasonable. While our findings do not determine if septins and RhoA directly interact or require intermediate effectors, we found consistent septin accumulation in regions of local RhoA activation. These data fit with other recent findings of RhoA regulating septin accumulation at the membrane of migrating border cells in *Drosophila* (Gabbert *et al.*, 2023), and with SEPT9 activating RhoA at sites of mitochondrial fission (Shannon *et al.*, 2025). Together, these findings suggest a more extensive role for RhoA in regulating septins.

That the septin response to RhoA is independent of anillin is somewhat surprising. Anillin is a scaffolding protein that binds directly to RhoA, septins, actin, myosin, and the plasma membrane, making it a reasonable candidate to mediate this interaction (Hickson and O'Farrell, 2008). During cytokinesis, RhoA binding to anillin is a prerequisite for septin binding, and the resulting structure facilitates contractile ring closure (Carim and Hickson, 2023). Anillin expression, however, is dependent on the cell cycle (Field and Alberts, 1995; Zhao and Fang, 2005; Mahdessian *et al.*, 2021), and we see little anillin present in our fibroblast cell line during interphase (Figure 4). This suggests that additional

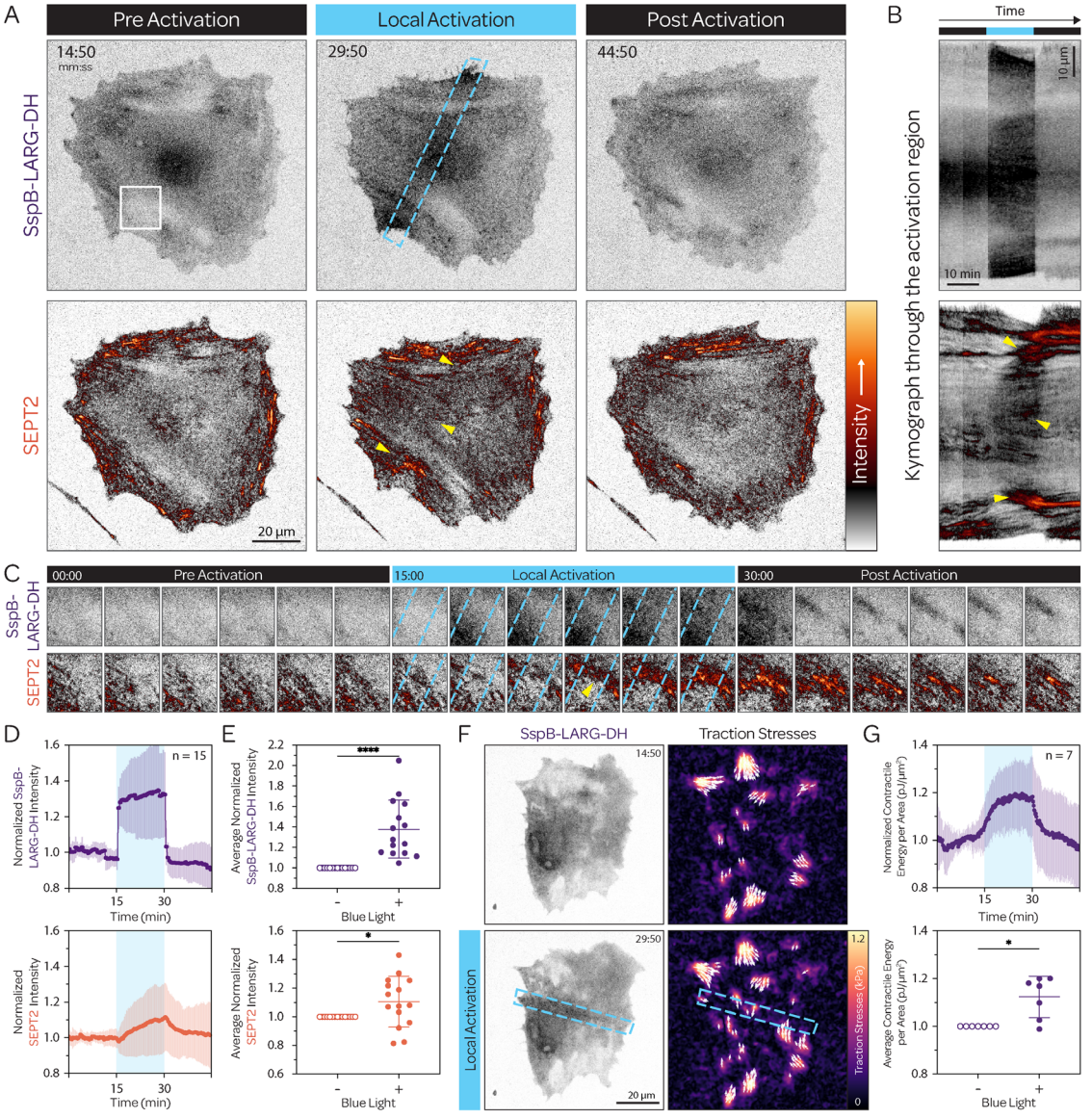

FIGURE 5: Local RhoA activation induces septin accumulation. (A) Representative images of SEPT2-Halo fibroblast, stably expressing Stargazin-mTurq2-LOV2-SsrA and transiently expressing mScarlet-SspB-LARG-DH. Local blue light stimulation (blue dashed box, top row) induces rapid mScarlet-SspB-LARG membrane recruitment, followed by septin accumulation. Both signals dissipate when blue light is turned off (refer to Supplemental Movie S8). (B) A kymograph through the activation region shows increased LARG-DH and SEPT2 intensities during the activation period. (D) Series of insets, white box in (A), showing recruitment of LARG-DH and SEPT2 in the activation region (between the two blue dashed lines). (D) Normalized mScarlet-SspB- LARG and SEPT2-Halo intensities (mean ± SD) in the region of RhoA activation are plotted over time, with activation periods indicated by the blue background. (E) Scatter plots of average intensity changes in the activation region between the 50 s pre-activation and the final 50 s of activation per cell. (F) Representative images of a fibroblast expressing the mScarlet-SspB- LARG-DH and the associated traction maps before and during local activation of RhoA (blue dashed box; refer to Supplemental Movie S9). (G) Average measurements of the normalized total contractile work per area performed by cells, and scatter plots comparing the contractile work per area before and during activation (mean ± SD). * and **** indicate $p \leq 0.05$ and ≤ 0.0001.

pathways exist to connect RhoA and septins outside those that are active during cytokinesis.

The specific mechanism by which RhoA influences septin organization remains unclear. The fact that the septin response builds slowly during local activation hints that it is likely not a direct interaction with RhoA, as the recruitment of the GEF happens almost immediately (Figure 5C). Our MLCK data indicate that downstream myosin-based force production alone is also insufficient (Figure 3). While RhoA stimulates actin polymerization via formins (Supplemental Figure S2B), septins only decorate a subpopulation of stress fibers in the cell (Figure 1) and are often absent from other regions with increased actin polymerization, such as the lamellipodia or filopodia. Therefore, actin polymerization alone also appears insufficient for septin recruitment, and additional signaling components are likely required. It is possible that the combination of RhoA-driven actin polymerization and myosin 2 contractility creates

a contractile network that is favorable for septin enrichment, consistent with the parallels drawn to the contractile ring. More probably, additional downstream RhoA effectors are aiding in septin recruitment, as is the case with Cdc42. Potential mediators could also depend on the cell cycle, which could explain some of the variation we see in the magnitude of the septin response. Septins have also been identified in several proteomic screens related to focal adhesions and other actomyosin structures (Schiller *et al.*, 2011; Horton *et al.*, 2015; Hecht *et al.*, 2019; Brock *et al.*, 2025), and future work will be required to whittle these lists down to a manageable number of potential targets. Additional experiments combining pharmacological inhibitors or multiple optogenetic targets to simultaneously activate RhoA while inhibiting downstream effectors could also offer potential clues into this mechanism.

In summary, this work demonstrates the power of optogenetic switches and activation in deciphering biochemical signaling within cells. Our data reveal a role for RhoA in reorganizing septin localization in response to RhoA activity outside of cell division. Furthermore, while septins do not appear to be directly responding to increases in myosin activity or contractility, their positioning on actin stress fibers and dynamic ability to reorganize in the cytoskeleton suggest that they may have other potential roles to play in mechanotransduction.

MATERIALS AND METHODS

Request a protocol through *Bio-protocol*

Cell culture and transfection

Mouse embryonic fibroblasts (MEFs) were a kind gift of Mary Beckerle's laboratory (University of Utah). HEK293T cells (CRL-3216; ATCC) were used to prepare the lentivirus. Cells were cultured in Dulbecco's modified Eagle's medium (10013CV; Corning), supplemented 10% FBS (10437-028, Life Technologies), 1% antibiotic-antimycotic (30004CI; Corning), and 5 µg/mL prophylactic plasmocin (ant-mpp; Invivogen) at 37°C in 5% CO_2. All cells were grown on uncoated plastic tissue culture dishes and plated on #1.5 glass-bottom dishes (Cellvis) or coverslips (Corning) for imaging.

At 16–20 hr before LARG-DH and 40–44 hr before NM2A and MLCK experiments, 100–125k MEF cells were transfected with the relevant plasmids, using the Neon Electroporation system (Thermo Fisher Scientific) with 3 × 20 ms pulses of 1000V and 4 µg total DNA in a 100 µl reaction. Cells were incubated with 100 nM Janelia Fluor JFX554 (HT030; Promega) or Janelia Fluor 646 (HT106A; Promega)/JFX650 HaloTag ligand (HT1070; Promega) overnight and washed out three times with PBS before imaging in media to visualize RhoA biosensor and Halo-tagged septin, respectively.

Generation of CRISPR knock-in cell lines

SEPT2-Halo knock-in cells were derived from parental fibroblasts using CRISPR/Cas9. We generated pSpCas9(BB)-2A- Puro (PX459) V2.0 (Plasmid #62988; Addgene) with target sequence 5′-AAACTTCATCAATAACCCGC-3′ using established protocols (Ran *et al.*, 2013). To generate donor plasmids, pUC57 was digested with EcoR1 and Stu1 and purified. A four-piece Gibson assembly was then performed with three gBlocks (IDT): (1) a 794 bp 5′HDR of genomic sequence immediately upstream of the endogenous start codon, (2) HaloTag with an 18 amino acid GS-rich linker, (3) an 802 bp 3′HDR of genomic sequence immediately downstream of the endogenous start codon with a silent PAM site mutation. Fibroblasts were transfected with donor and target-Cas9 plasmids and single-cell sorted. Individual clones were evaluated for knock-in via Western blotting and microscopy (Utgaard *et al.*, 2026).

Expression vectors and molecular cloning

pSspB-mApple-NM2A and pSspB-EGFP-LARG-DH were previously described (Quintanilla *et al.*, 2024). dimericTomato-1xwGBD was a gift from Dorus Gadella (Plasmid #176099; Addgene; Mahlandt *et al.*, 2023a). pShuttle-CMV-Halo-AHPH ("RhoA biosensor") was generated by digesting pShuttle-CMV (Plasmid #16403; Addgene; He *et al.*, 1998) with Not1 and inserting PCR-amplified Halo-Tag and AHPH from pEGFP-RhoA Biosensor (Plasmid #68026; Addgene; Piekny and Glotzer, 2008) using Gibson cloning. pmScarlet-SspB-LARG-DH was generated in two steps using pLV-GFP (Plasmid #25999; Addgene; Beronja *et al.*, 2010) as a backbone. We used Gibson cloning to sequentially replace GFP with mScarlet, then inserted SspB-LARG-DH PCR amplified from mCherry-NES-SspB-LARG-DH-P2A-iLIDcaax (Plasmid #173870; Addgene; Inaba *et al.*, 2021). To generate pSspB-LARG-iRFP720 plasmid, SspB-LARG was inserted into piRFP720-N1 vector (Plasmid #45461; Addgene; Shcherbakova and Verkhusha, 2013) using the AgeI and HindIII restriction sites. To generate a photorecruitable MLCK catalytic domain (pSspB-mApple-MLCK-cat), we used Gibson cloning to insert the human MLCK (NM 053025.4) catalytic domain corresponding to AA G1424 - K1770 into pSspb-mApple-NM2A (Quintanilla *et al.*, 2024) following removal of NM2A with HindIII and Spe1. The linker between mApple and MLCK catalytic domain is YSDLELKL. To generate a myosin RLC iLID anchor (pLV-MYL12B-mTurqoise2-iLID) we used Gibson cloning to replace ADRB2 in pLV-ADRB2-mTurqoise2-iLID (Plasmid #161002; Addgene; Natwick and Collins, 2020) using BamH1 restriction sites with the human MYL12B coding sequence from NM 033546.4. All constructs were verified by full-plasmid sequencing.

Stable cell lines

HEK293T cells were transfected using LipoD293 (SL100668; Signagen) and the accompanying lentivirus generation transfection protocol. Briefly, HEK293T cells were plated in 6-cm dishes and grown to 80%–90% confluence. Approximately 1 hr before transfection, the media was changed. The transfection complex was created with LipoD293, packaging plasmid psPax (Plasmid #12260; Addgene), envelope plasmid pmD2.G (Plasmid #12259; Addgene), and lentiviral construct pLV-Stargazin- mTurquoise2-iLID (Plasmid #161001; Addgene), and added drop-wise to the dish. Media was changed 24 hr after transfection and collected at 48 and 72 hr. Viral media was centrifuged at 1600 g for 5 min. A 50% confluent 6 cm of cells (wild-type and septin knock-in MEFs) were transduced with viral media supernatant. Viral media was removed after 48 hr. At 3 d post viral transduction, positive cells were selected using 2 µg/mL blasticidin (ant-bl-1; Invivogen).

Live-cell imaging

Cells were rinsed with PBS before imaging and replenished with fresh culture media. All imaging was performed at 37°C with 5% CO_2 on an Axio Observer 7 inverted microscope (Zeiss) attached to a W1 Confocal Spinning Disk (Yokogawa) with Mesa field flattening (Intelligent Imaging Innovations), a motorized X, Y stage (ASI), and a Prime 95B sCMOS (Photometrics) camera. Illumination was provided by a TTL-triggered multifiber laser launch (Intelligent Imaging Innovations) consisting of six diode laser lines (405, 445, 488, 514, 561, and 640 nm) and all matching requisite filters using a 63X, 1.4 NA Plan Apochromat objective (Zeiss). Temperature and humidity were maintained using a Bold Line full enclosure incubator

(Oko Labs). The microscope was controlled using Slidebook 6 Software (Intelligent Imaging Innovations). All imaging was performed as single confocal slices. Images were captured every 10 s, except for SspB-mApple-MLCK, mScarlet-SspB-LARG-DH, iRFP720-SspB-LARG-DH, and Sspb-mApple-NM2A constructs, which were imaged every 30 s to limit photobleaching. Images displayed as inverted grayscale or with a custom look-up table ("MQ div-autumn"; Quintanilla *et al.*, 2024) downloadable at https://sites.imagej.net/NeuroCyto-LUTs/ and modifiable via https://github.com/m-a-q.

Fixed imaging

Blebbistatin and Rho Inhibitor treatment. MEFs were plated on #1.5 glass coverslips (Corning) 24 hr before treatment. Cells were treated with vehicle, 20 µm of the myosin inhibitor (-)- blebbistatin (856925-71-8; Cayman Chemical) for 1 hr, or 2 µg/mL the Rho Inhibitor CT04 (CT04-A; Cytoskeleton Inc) for 3 hr. For dual treatment with both blebbistatin and CT04, cells were first incubated with CT04 for 2 hr before adding blebbistatin and allowing them to incubate for 1 hr to keep the total time of each treatment consistent between conditions. After treatment, the cell culture media was gently rinsed with cytoskeleton buffer (CB; 19.52 g MES [0.1 M], 6.10 g MgCl2 [0.03 M], 102.88 g KCl [1.38 M], 7.6 g EGTA [0.02 M]) and replaced with a fixing and blocking solution (0.15 g BSA, 2.5 mL 16% paraformaldehyde solution, 50 µl Triton, and 7.5 mL CB) for 1 hr at room temperature on a rocker. Cells were washed 3 × 5 min with 1x PBS before incubating overnight at 4°C in primary antibody for SEPT2 (11397-1-AP; Proteintech) diluted 1:300 in antibody solution (0.15 g BSA, 50 µl Triton, and 10 mL CB). The next day, coverslips were washed 3 × 5 min with 1x PBS before incubating for 1 hr in the dark in rabbit fluorescent secondary antibody (A11036; ThermoFisher Scientific) diluted 1:1000 in antibody solution with 1:1000 Atto-Phalloidin (65906-10NMOL; Sigma-Aldrich). A final PBS wash was performed (3 × 5 min) before mounting the cells on a glass slide with ProLong Glass Antifade Mountant (P36980; ThermoFisher Scientific). Cells were imaged 24 hr after mounting. For analysis, the top 2% of SEPT2-intensity pixels were selected, and stress fiber localization was scored in a binary manner based on whether these pixels overlapped with the actin stress fibers. For scoring, images of all treatments were randomly ordered, and scoring was performed blindly by two independent researchers. The percentage recorded for each treatment was the average of the two independent scores.

Anillin staining. Local RhoA activation was performed for 15 min, and then ice-cold methanol was added to the coverslip within seconds after the last blue light exposure while the sample was still on the microscope stage. Fixation for 20 min at 37°C was followed by three PBS washes. Permeabilization was carried out for 5 min in a buffer containing 0.5% Triton X-100 in CB. For blocking, cells were incubated with 1.5% BSA in CB for 1 hr at room temperature on a rocker. Cells were then incubated overnight at 4°C with polyclonal anti-anillin sera (1:500; Gift of Michael Glotzer, University of Chicago). The next day, cells were washed three times with PBS and incubated with secondary antibody (goat anti-rabbit Alexa Fluor 647; 1:1000; #A32733; ThermoFisher Scientific) for 1 hr at room temperature. All post-fixation incubations were performed on a rocker. The average intensity within the activation region was obtained for both LARG and anti-anillin and then normalized to the average intensity in an unactivated region.

iLID photorecruitment and analysis

Before each time lapse, the potential cell was imaged with a test time lapse consisting of 640 nm/561 nm/445 nm excitation captures taken sequentially, and then repeated after 5 s (Supplemental Figure S1). If the anchor and its binding partner were both expressed in the cell, we would see relocation of the binding partner to the anchor following the 445 nm excitation. Once the expression of both components was confirmed, the cell was kept in the dark for at least 5 min to allow the two components to fully dissociate. During this time, a box with a width of ~5–10 µm was drawn across the ventral surface of a cell in Slidebook 6. We then proceeded with steady state imaging for 5 (Figures 4; Supplemental Figure SS2) or 15 min (Figures 2, 3, and 5), before the local recruitment region was illuminated with a 405 nm laser for the same duration (5 or 15 min) at 6 µW, followed by additional period of imaging (5 or 15 min) without local stimulation. Illumination of the local recruitment region was repeated every 10 s before the imaging at that time point. Cell counts are provided in the figures.

Analysis was performed using Python. Cell masks for each cell were generated in FIJI by thresholding the signal in the 561 nm channel. Images were corrected for photobleaching and flat-field. Following correction, the intensity within the region of activation (region extracted from Slidebook6) and cell mask was calculated for each image/frame. This intensity was normalized to the mean intensity of the frames before photo recruitment and plotted as normalized intensity over time. Where necessary, intensities were normalized to a non-activated region to account for shifts in focus.

Traction force microscopy and analysis

Traction force microscopy was performed as previously described (Schmitt *et al.*, 2024). Coverslips were prepared by incubating with a 2% solution of 3-aminopropyltrimethyoxysilane (313255000; Acros Organics) diluted in isopropanol, followed by fixation in 1% glutaraldehyde (16360; Electron Microscopy Sciences) in ddH_2O. Polyacrylamide gels (shear modulus: 8.6 kPa—final concentrations of 7.5% acrylamide (1610140; Bio-Rad) and 0.3% bis-acrylamide (1610142; Bio-Rad)) were embedded with 0.04 µm fluorescent microspheres (F8789; Invitrogen) and polymerized on the activated glass coverslips for 1 hr at room temperature. After polymerization, gels were rehydrated for at least 60 min. To cross-link the gels with fibronectin, gels were treated with the cross-linker Sulfo-Sanpah (22589; Pierce Scientific), photoactivated with UV light for 5 min, and then rinsed thoroughly with ddH_2O. Gels were then incubated with 40 µl of 1 mg/mL human plasma fibronectin (FC010; Millipore) for 1 hr at room temperature. Following fibronectin cross-linking, transfected cells were plated on the gels and allowed to spread overnight. Images were taken of both the cells and the underlying fluorescent beads. Following imaging, cells were detached from the gel using 0.05% SDS (L22010; Research Products International Corp), and a reference image of the fluorescent beads in the unstrained gel was taken.

Analysis of traction forces was performed using code written in Python (available at https://github.com/OakesLab/TFM) according to previously described approaches (Huang *et al.*, 2019; Schmitt *et al.*, 2024). Before processing, images were flat-field and photobleach corrected and aligned to the reference bead image with the cell detached. Other acquired channels were shifted using the same alignment measurements from the bead channel. Displacements in the beads were calculated using an optical flow algorithm in OpenCV (Open Source Computer Vision Library, https://github.com/itseez/opencv) with a window size of eight pixels. Traction stresses were calculated using the Fourier Transform Traction Cytometry (FTTC) approach with a regularization parameter of 7.9×10^{-7}. The strain energy was calculated by summing one-half the product of the strain and traction vectors in the region under the

cell and normalizing by the cell area as measured from the cell mask (Oakes *et al.*, 2014).

Statistical analysis

Statistical analyses were performed on GraphPad Prism using the nonparametric Wilcoxon matched-pairs signed-rank test. *P*-values < 0.05 were considered statistically significant. Details about sample size and *p*-values are included in the figure legends.

ACKNOWLEDGMENTS

We thank the rest of the Oakes and Beach laboratories at Loyola University Chicago, and Elias Spiliotis at the University of Virginia, for many helpful discussions. We thank Dr. Stefano Sala for assistance in swapping the fluorophores to create the iRFP720-SspB-LARG-DH construct. This work was supported in part by NIH NIGMS grant R35-GM138183 to JRB, and NSF CAREER award #2000554 and NIH NIGMS grant R01-GM148644 to PWO.

REFERENCES

Ageta-Ishihara N, Kinoshita M (2021). Developmental and postdevelopmental roles of septins in the brain. Neurosci Res 170, 6–12.

Bai X, Bowen JR, Knox TK, Zhou K, Pendziwiat M, Kuhlenbäumer G, Sindelar CV, Spiliotis ET (2013). Novel septin 9 repeat motifs altered in neuralgic amyotrophy bind and bundle microtubules. J Cell Biol 203 (6), 895–905.

Bement WM, Leda M, Moe AM, Kita AM, Larson ME, Golding AE, Pfeuti C, Su KC, Miller AL, Goryachev AB, von Dassow G (2015). Activator-inhibitor coupling between rho signalling and actin assembly makes the cell cortex an excitable medium. Nat Cell Biol 17 (11), 1471–1483.

Beronja S, Livshits G, Williams S, Fuchs E (2010). Rapid functional dissection of genetic networks via tissue-specific trans- duction and RNAi in mouse embryos. Nat Med 16 (7), 821–827.

Bhadriraju K, Yang M, Alom Ruiz S, Pirone D, Tan J, Chen CS (2007). Activation of ROCK by RhoA is regulated by cell adhesion, shape, and cytoskeletal tension. Exp Cell Res 313 (16), 3616–3623.

Bridges AA, Jentzsch MS, Oakes PW, Occhipinti P, Gladfelter AS (2016). Micron-scale plasma membrane curvature is recog- nized by the septin cytoskeleton. J Cell Biol 213 (1), 23–32.

Brock K, Alpha KM, Brennan G, De Jong EP, Luke E, Turner CE (2025). A comparative analysis of paxillin and Hic-5 proximity interactomes. Cytoskeleton (Hoboken, NJ) 82 (1-2), 12–31.

Calvo F, Ranftl R, Hooper S, Farrugia AJ, Moeendarbary E, Bruckbauer A, Batista F, Charras G, Sahai E (2015). Cdc42EP3/BORG2 and septin network enables mechano-transduction and the emergence of cancer-associated fibroblasts. Cell Rep 13 (12), 2699–2714.

Calvo F, Ranftl R, Hooper S, Sahai E (2016). YAP, Cdc42EP3 and septins modulate mechano-transduction and the emergence of cancer-associated fibroblasts. Eur J Cancer 61, S69–S70.

Cannon KS, Woods BL, Crutchley JM, Gladfelter AS (2019). An amphipathic helix enables septins to sense micrometer-scale membrane curvature. J Cell Biol 218, 1128-1137.

Carim SC, Hickson GRX (2023). The Rho1 GTPase controls anillo-septin assembly to facilitate contractile ring closure during cytokinesis. iScience 26 (6), 106903.

Cavini IA, Leonardo DA, Rosa HVD, Castro DKSV, D'Muniz Pereira H, Valadares NF, Araujo APU, Garratt RC (2021). The structural biology of septins and their filaments: an update. Front Cell Dev Biol 9, 765085.

Chandrasekar S, Beach JR, Oakes PW (2023). Shining a light on RhoA: optical control of cell contractility. Int J Biochem Cell Biol 161, 106442.

de Beco S, Vaidžiulytė K, Manzi J, Dalier F, di Federico F, Cornilleau G, Dahan M, Coppey M (2018). Optogenetic dissection of Rac1 and Cdc42 gradient shaping. Nat Commun 9 (1), 4816.

Delic S, Shuman B, Lee S, Bahmanyar S, Momany M, Onishi M (2024). The evolutionary origins and ancestral features of septins. Front Cell Dev Biol 12.

Devlin L, Okletey J, Perkins G, Bowen JR, Nakos K, Montagna C, Spiliotis ET (2021). Proteomic profiling of the oncogenic septin 9 reveals isoform-specific interactions in breast cancer cells. Proteomics e2100155.

Dolat L, Hu Q, Spiliotis ET (2014a). Septin functions in organ system physiology and pathology. Biol Chem 395 (2), 123–141.

Dolat L, Hunyara JL, Bowen JR, Karasmanis EP, Elgawly M, Galkin VE, Spiliotis ET (2014b). Septins promote stress fiber- mediated maturation of focal adhesions and renal epithelial motility. J Cell Biol 207 (2), 225–235.

Field CM, Alberts BM (1995). Anillin, a contractile ring protein that cycles from the nucleus to the cell cortex. J Cell Biol 131 (1), 165–178.

Füchtbauer A, Lassen LB, Jensen AB, Howard J, Quiroga AdS, Warming S, Sørensen AB, Pedersen FS, Füchtbauer EM (2011). Septin9 is involved in septin filament formation and cellular stability. Biol Chem 392 (8-9), 769–777.

Gabbert AM, Campanale JP, Mondo JA, Mitchell NP, Myers A, Streichan SJ, Miolane N, Montell DJ (2023). Septins regulate border cell surface geometry, shape, and motility downstream of Rho in *Drosophila*. Dev Cell 58, 1399-1413.e5.

Gladfelter AS, Bose I, Zyla TR, Bardes ESG, Lew DJ (2002). Septin ring assembly involves cycles of GTP loading and hydrolysis by Cdc42p. J Cell Biol 156 (2), 315–326.

Guilluy C, Garcia-Mata R, Burridge K (2011). Rho protein crosstalk: another social network? Trends Cell Biol 21 (12), 718–726.

Guntas G, Hallett RA, Zimmerman SP, Williams T, Yumerefendi H, Bear JE, Kuhlman B (2015). Engineering an improved light-induced dimer (iLID) for controlling the localization and activity of signaling proteins. Proc Natl Acad Sci USA 112 (1), 112–117.

Hagiwara A, Tanaka Y, Hikawa R, Morone N, Kusumi A, Kimura H, Kinoshita M (2011). Submembranous septins as relatively stable components of actin-based membrane skeleton. Cytoskeleton (Hoboken, NJ) 68 (9), 512–525.

Hartwell LH (1971). Genetic control of the cell division cycle in yeast. IV. Genes controlling bud emergence and cytokinesis. Exp Cell Res 69 (2), 265–276.

He TC, Zhou S, da Costa LT, Yu J, Kinzler KW, Vogelstein B (1998). A simplified system for generating recombinant aden- oviruses. Proc Natl Acad Sci USA 95 (5), 2509–2514.

Hecht M, Rösler R, Wiese S, Johnsson N, Gronemeyer T (2019). An interaction network of the human SEPT9 established by quantitative mass spectrometry. G3 9 (6), 1869–1880.

Hickson GR, O'Farrell PH (2008). Anillin: a pivotal organizer of the cytokinetic machinery. Biochem Soc Trans 36 (Pt 3), 439–441.

Horton ER, Byron A, Askari JA, Ng DHJ, Millon-Frémillon A, Robertson J, Koper EJ, Paul NR, Warwood S, Knight D, *et al.* (2015). Definition of a consensus integrin adhesome and its dynamics during adhesion complex assembly and disassembly. Nat Cell Biol 17 (12), 1577–1587.

Huang Y, Schell C, Huber TB, Ek ANAXIX, Hersch N, Merkel R, Gompper G, Sabass B (2019). Traction force microscopy with optimized regularization and automated Bayesian parameter selection for comparing cells. Sci Rep 9 (1), 1–16.

Inaba H, Miao Q, Nakata T (2021). Optogenetic control of small GTPases reveals RhoA mediates intracellular calcium signal- ing. J Biol Chem 296.

Jaffe AB, Hall A (2005). Rho GTPases: biochemistry and biology. Annu Rev Cell Dev Biol 21, 247–269.

Jaiswal M, Gremer L, Dvorsky R, Haeusler LC, Cirstea IC, Uhlenbrock K, Ahmadian MR (2011). Mechanistic insights into specificity, activity, and regulatory elements of the regulator of G-protein signaling (RGS)-containing Rho-specific guanine nucleotide exchange factors (GEFs) p115, PDZ-RhoGEF (PRG), and leukemia-associated RhoGEF (LARG). J Biol Chem 286 (20), 18202–18212.

Jiao F, Cannon KS, Lin YC, Gladfelter AS, Scheuring S (2020). The hierarchical assembly of septins revealed by high-speed AFM. Nat Commun 11 (1), 5062.

Joberty G, Perlungher RR, Sheffield PJ, Kinoshita M, Noda M, Haystead T, Macara IG (2001). Borg proteins control septin organization and are negatively regulated by Cdc42. Nat Cell Biol 3 (10), 861–866.

Joo E, Surka MC, Trimble WS (2007). Mammalian SEPT2 is required for scaffolding nonmuscle myosin II and its kinases. Dev Cell 13 (5), 677–690.

Kinoshita M, Field CM, Coughlin ML, Straight AF, Mitchison TJ (2002). Self- and actin-templated assembly of mammalian septins. Dev Cell 3 (6), 791–802.

Kramer MM, Lataster L, Weber W, Radziwill G (2021). Optogenetic approaches for the spatiotemporal control of signal transduction pathways. Int J Mol Sci 22 (10).

Lam M, Calvo F (2018). Regulation of mechanotransduction: emerging roles for septins. Cytoskeleton 76 (1), 115–122.

Lawson CD, Ridley AJ (2018). Rho GTPase signaling complexes in cell migration and invasion. J Cell Biol 217 (2), 447–457.

Longtine MS, DeMarini DJ, Valencik ML, Al-Awar OS, Fares H, De Virgilio C, Pringle JR (1996). The septins: roles in cytokinesis and other processes. Curr Opin Cell Biol 8 (1), 106–119.
Mahdessian D, Cesnik AJ, Gnann C, Danielsson F, Stenström L, Arif M, Zhang C, Le T, Johansson F, Schutten R, *et al.* (2021). Spatiotemporal dissection of the cell cycle with single-cell proteogenomics. Nature 590 (7847), 649–654.
Mahlandt EK, Kreider-Letterman G, Chertkova AO, Garcia-Mata R, Goedhart J (2023a). Cell-based optimization and charac- terization of genetically encoded location-based biosensors for Cdc42 or rac activity. J Cell Sci 136 (10).
Mahlandt EK, Palacios Martínez S, Arts JJ, Tol S, van Buul JD, Goedhart J (2023b). Opto-RhoGEFs, an optimized optogenetic toolbox to reversibly control Rho GTPase activity on a global to subcellular scale, enabling precise control over vascular endothelial barrier strength. eLife 12, RP84364.
Martins CS, Taveneau C, Castro-Linares G, Baibakov M, Buzhinsky N, Eroles M, Milanovic´ V, Omi S, Pedelacq JD, Iv F, *et al.* (2023). Human septins organize as octamer-based filaments and mediate actin-membrane anchoring in cells. J Cell Biol 222 (3).
Mavrakis M, Azou-Gros Y, Tsai FC, Alvarado J, Bertin A, Iv F, Kress A, Brasselet S, Koenderink GH, Lecuit T (2014). Septins promote F-actin ring formation by crosslinking actin filaments into curved bundles. Nat Cell Biol 16 (4), 322–334.
Menon MB, Sawada A, Chaturvedi A, Mishra P, Schuster-Gossler K, Galla M, Schambach A, Gossler A, Förster R, Heuser M, *et al.* (2014). Genetic deletion of sept7 reveals a cell type-specific role of septins in microtubule destabilization for the completion of cytokinesis. PLoS Genetics 10 (8), e1004558.
Mostowy S, Cossart P (2012). Septins: the fourth component of the cytoskeleton. Nat Rev Mol Cell Biol 13 (3), 183–194.
Müller PM, Rademacher J, Bagshaw RD, Wortmann C, Barth C, van Unen J, Alp KM, Giudice G, Eccles RL, Heinrich LE, *et al.* (2020). Systems analysis of RhoGEF and RhoGAP regulatory proteins reveals spatially organized RAC1 signalling from integrin adhesions. Nat Cell Biol 22 (4), 498–511.
Nakazawa K, Kumar G, Chauvin B, Di Cicco A, Pellegrino L, Trichet M, Hajj B, Cabral J, Sain A, Mangenot S, Bertin A (2023). A human septin octamer complex sensitive to membrane curvature drives membrane deformation with a specific mesh-like organization. J Cell Sci 136 (11), jcs260813.
Natwick DE, Collins SR (2020). Optimized iLID membrane anchors for local optogenetic protein recruitment. ACS Synth Biol 10 (5), 1009–1023.
Oakes PW, Banerjee S, Marchetti MC, Gardel ML (2014). Geometry regulates traction stresses in adherent cells. Biophys J 107 (4), 825–833.
Oakes PW, Wagner E, Brand CA, Probst D, Linke M, Schwarz US, Glotzer M, Gardel ML (2017). Optogenetic control of RhoA reveals zyxin-mediated elasticity of stress fibres. Nat Commun 8, 15817.
Okada H, Chen X, Wang K, Marquardt J, Bi E (2023). Bni5 tethers myosin-II to septins to enhance retrograde actin flow and the robustness of cytokinesis. bioRxiv 2023.11.07.566094.
O'Neill PR, Kalyanaraman V, Gautam N (2016). Subcellular optogenetic activation of Cdc42 controls local and distal signaling to drive immune cell migration. Mol Biol Cell 27 (9), 1442–1450.
Palander O, El-Zeiry M, Trimble WS (2017). Uncovering the roles of septins in cilia. Front Cell Dev Biol 5, 36.
Peterson EA, Petty EM (2010). Conquering the complex world of human septins: implications for health and disease. Clin Genet 77 (6), 511–524.
Piekny AJ, Glotzer M (2008). Anillin is a scaffold protein that links RhoA, actin, and myosin during cytokinesis. Curr Biol 18 (1), 30–36.
Quintanilla MA, Patel H, Wu H, Sochacki KA, Chandrasekar S, Akamatsu M, Rotty JD, Korobova F, Bear JE, Taraska JW, *et al.* (2024). Local monomer levels and established filaments potentiate non-muscle myosin 2 assembly. J Cell Biol 223 (4), e202305023.
Ran FA, Hsu PD, Wright J, Agarwala V, Scott DA, Zhang F (2013). Genome engineering using the CRISPR-Cas9 system. Nat Protoc 8 (11), 2281–2308.
Ridley AJ, Hall A (1992). The small GTP-binding protein rho regulates the assembly of focal adhesions and actin stress fibers in response to growth factors. Cell 70 (3), 389–399.
Röseler S, Sandrock K, Bartsch I, Busse A, Omran H, Loges NT, Zieger B (2011). Lethal phenotype of mice carrying a Sept11 null mutation. Biol Chem 392 (8-9), 779–781.
Salameh J, Cantaloube I, Benoit B, Poüs C, Baillet A (2021). Cdc42 and its BORG2 and BORG3 effectors control the subcel- lular localization of septins between actin stress fibers and microtubules. Curr Biol 31 (18), 4088–4103.e5.
Schiller HB, Friedel CC, Boulegue C, Fässler R (2011). Quantitative proteomics of the integrin adhesome show a myosin II-dependent recruitment of LIM domain proteins. EMBO Rep 12 (3), 259–266.
Schmidt K, Nichols BJ (2004). Functional interdependence between septin and actin cytoskeleton. BMC Cell Biol 5 (1), 43.
Schmitt MS, Colen J, Sala S, Devany J, Seetharaman S, Caillier A, Gardel ML, Oakes PW, Vitelli V (2024). Machine learning interpretable models of cell mechanics from protein images. Cell 187 (0), 481–494.
Seze JD, Bongaerts M, Boulevard B, Coppey M (2023). Optogenetic control of a GEF of RhoA uncovers a signaling switch from retraction to protrusion. eLife 12.
Shannon R, Balachandran Y, Wang X, Boutry M, Xie H, Kim PK, Trimble WS (2025). SEPTIN9 locally activates the RhoGEF ARHGEF18 to promote early stages of mitochondrial fission. J Cell Biol 224 (10), e202406017.
Shcherbakova DM, Verkhusha VV (2013). Near-infrared fluorescent proteins for multicolor in vivo imaging. Nat Methods 10 (8), 751–754.
Shindo A, Wallingford JB (2014). PCP and septins compartmentalize cortical actomyosin to direct collective cell movement. Science 343 (6171), 649–652.
Shizaki T, Naito M, Fujisawa K, Maekawa M, Watanabe N, Saito Y, Narumiya S (1997). Rho-associated coiled-coil forming protein kinase, works downstream rho induces focal adhesions. FEBS Lett 160, 118–124.
Smith C, Dolat L, Angelis D, Forgacs E, Spiliotis ET, Galkin VE (2015). Septin 9 exhibits polymorphic binding to F-actin and inhibits myosin and cofilin activity. J Mol Biol 427 (20), 3273–3284.
Spiliotis ET (2018). Spatial effects - site-specific regulation of actin and microtubule organization by septin GTPases. J Cell Sci 131 (1).
Sturgess W, Packirisamy S, Geneidy R, Nordenfelt P, Swaminathan V (2024). Extracellular matrix-dependent regulation of Septin 7 in focal adhesions promotes mechanosensing and functional response in fibroblasts. iScience 111355.
Svitkina T (2018). The actin cytoskeleton and actin-based motility. Cold Spring Harb Perspect Biol 10 (1), a018267.
Tomasso MR, Mehetre PD, Nagarajan P, Ravi R, Byrnett J, Brinckman E, Magliozzi J, Goode BL, Padrick SB (2025). Cdc42EP3-bound septin scaffolds promote actin polymerization. J Biol Chem 301 (3).
Tooley AJ, Gilden J, Jacobelli J, Beemiller P, Trimble WS, Kinoshita M, Krummel MF (2009). Amoeboid T lymphocytes require the septin cytoskeleton for cortical integrity and persistent motility. Nat Cell Biol 11 (1), 17–26.
Tran AT, Wisniewski EO, Mistriotis P, Stoletov K, Parlani M, Amitrano A, Ifemembi B, Lee SJ, Bera K, Zhang Y, *et al.* (2025). Cytoplasmic anillin and Ect2 promote RhoA/myosin II-dependent confined migration and invasion. Nat Mater 24 (9), 1476–1488.
Utgaard ME, Caillier A, Chandrasekar S, Tidei JJ, Balasubramanian H, Lee RM, Puls O, Khuon S, Aaron J, Chew TL, *et al.* (2026). Mechanically-induced Septin Networks Protect Nuclear Integrity. bioRxiv 2026.01.20.700414.
Vadnjal N, Nourreddine S, Lavoie G, Serres M, Roux PP, Paluch EK (2022). Proteomic analysis of the actin cortex in interphase and mitosis. J Cell Sci 135 (16), jcs259993.
Valon L, Marín-Llauradó A, Wyatt T, Charras G, Trepat X (2017). Optogenetic control of cellular forces and mechanotrans- duction. Nat Commun 8, 14396.
Van Ngo H, Mostowy S (2019). Role of septins in microbial infection. J Cell Sci 132 (9), jcs226266.
Wagner E, Glotzer M (2016). Local RhoA activation induces cytokinetic furrows independent of spindle position and cell cycle stage. J Cell Biol 213 (6), 641–649.
Watanabe N, Madaule P, Reid T, Ishizaki T, Watanabe G, Saito Y, Nakao K, Jockusch BM, Narumiya S (1997). p140mDia, mammalian homolog drosophila diaphanous, target protein rho small GTPase ligand profilin. EMBO J 16, 3044–3056.
Weems AD, Welf ES, Driscoll MK, Zhou FY, Mazloom-Farsibaf H, Chang BJ, Murali VS, Gihana GM, Weiss BG, Chi J, *et al.* (2023). Blebs promote cell survival by assembling oncogenic signalling hubs. Nature 615 (7952), 517–525.
Woods BL, Gladfelter AS (2021). The state of the septin cytoskeleton from assembly to function. Curr Opin Cell Biol 68, 105–112.
Zhao W, Fang G (2005). Anillin is a substrate of anaphase-promoting complex/cyclosome (APC/C) that controls spatial contractility of myosin during late cytokinesis*[boxs]. J Biol Chem 280 (39), 33516–33524.
Zhovmer AS, Manning A, Smith C, Nguyen A, Prince O, Sáez PJ, Ma X, Tsygankov D, Cartagena-Rivera AX, Singh NA, *et al.* (2024). Septins provide microenvironment sensing and cortical actomyosin partitioning in motile amoeboid T lymphocytes. Sci Adv 10 (1), eadi1788.